

On-Chip, Dynamic, and Cryogenic Temperature Monitoring via PDMS Micro-Bead Coatings

Matthew Frenkel, Zhixiong Guo

Department of Mechanical and Aerospace Engineering, Rutgers, the State University of New Jersey, Piscataway, New Jersey 08854

Correspondence to: Z. Guo (E-mail: guo@jove.rutgers.edu)

Received 16 December 2015; accepted 22 January 2016; published online 22 February 2016

DOI: 10.1002/polb.24016

ABSTRACT: Polydimethylsiloxane (PDMS) microspheres/beads coated onto an electrical current-carrying wire are demonstrated for on-chip, dynamic, cryogenic temperature measurement via monitoring optical whispering-gallery mode (WGM) frequency shifts. PDMS is found to be capable of supporting WGM resonance at cryogenic temperatures down to 95 K, limited by the present lab-built cryogenic working environment. The effect of the polymeric sensor diameter on temperature sensitivity is explored and discussed. The sensors are tested for their real-

time temperature monitoring capabilities and accuracy in the cryogenic temperature regime of 95–140 K, and a comparison to a theoretical model, where the electrical resistivity of nichrome wire at cryogenic temperature is also experimentally determined, is examined. © 2016 Wiley Periodicals, Inc. *J. Polym. Sci., Part B: Polym. Phys.* **2016**, *54*, 1118–1124

KEYWORDS: coatings; cryogenic temperature; electrical resistivity; films; optical resonance; sensors

INTRODUCTION Optical resonances of whispering-gallery mode (WGM) devices have attracted increasing attention over the past two decades.^{1–9} The small mode volume, localized to the surface, of optical WGM resonators allows for considerable interaction with surrounding environment, and their intrinsically high-quality (Q) factor enables WGM-based sensors to exhibit extremely high-resolution.^{2–4} WGM resonators have found use in microlasers,¹ quantum electrodynamics,^{5,6} optical signal manipulation,^{7–9} etc. In particular, optical WGM sensors are being actively studied in a number of different detection and measurement applications. Examples included biological/chemical detection,^{10–16} humidity,¹⁷ pressure,¹⁸ and temperature monitoring,^{19–22} to name a few. The intrinsic high Q -factor of WGM-based sensors, in junction with the fact that the sensing principles are frequency, and not intensity based, enables high sensitivity and fine resolution measurement. Detection of single molecule and individual RNA viruses,^{11–13} pico-molar chemical residues,¹⁶ milli-newton force,¹⁸ and milli-kelvin temperature shifts have been reported in the literature.²⁰

Optical WGM temperature sensors were initially demonstrated at both room temperature and cryogenic regimes using fused silica microspheres,^{19–21} but polymer-based sensors have drawn a lot of consideration over the past few years. The low cost, ease of fabrication, and myriad of applications have generated a number of polymer-based sensor publications.^{23–25} He et al. analyzed thermal compensation in WGM resonators

coated with a layer of polydimethylsiloxane (PDMS).²⁶ Several studies of PDMS coating on thermal sensing then followed.^{27–29} Li et al.²⁸ thought about the concept of on-chip sensing based on WGM resonance. The actual demonstration of on-chip real-time operation measurement was carried out by Frenkel et al.,²⁹ in which a PDMS-based WGM resonator was fabricated directly onto an electrical current-carrying wire and be used for dynamic temperature monitoring of the wire's temperature due to Joule heating. WGM resonances of the coated PDMS composite sensors were determined jointly by the thermal effects of both the PDMS coating and core material. Recently, Ali et al. considered polymeric microspheres to electrical field measurement.⁹

In this article, we look to expand on our previous work with PDMS composite sensors at room temperature to cryogenic temperature because of wide cryogenic applications.²⁹ For example, it is paramount to determine the critical temperature of superconductivity. Because of the ease in fabrication and cost-effectiveness using PDMS-coated sensors, it is worthy of exploring the feasibility and capability of PDMS-based WGM resonators within the cryogenic temperature regime. We will explore the effect of PDMS coating thickness on the sensitivity of cryogenic temperature measurement, as well as, the accuracy of the sensor for dynamic cryogenic temperature monitoring. To the author's knowledge this is the first study of PDMS-based WGM resonance at cryogenic temperatures, as

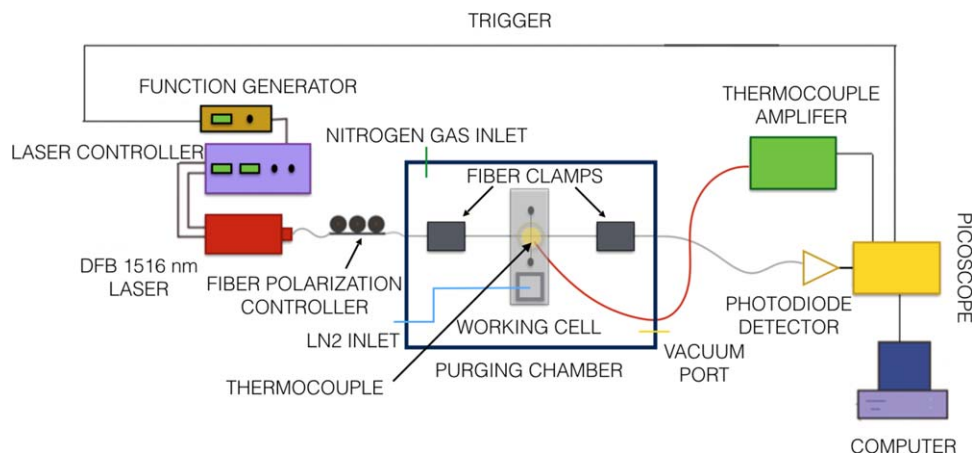


FIGURE 1 Experimental setup. [Color figure can be viewed in the online issue, which is available at wileyonlinelibrary.com.]

well as, the first attempt to use polymeric sensors for dynamic on-chip temperature monitoring at these low temperatures.

EXPERIMENTAL

The experimental setup used in this study is adapted from a previous study of the present authors.²⁹ The setup consists of five key components: the working electric component, the WGM composite sensor, the purging chamber, the cryogenic working cell, and the data acquisition system. The working electric component, fabrication of PDMS-coated WGM sensor, and data acquisition system were detailed in Frenkel et al.²⁹; the only notable difference, among these three components, is that the fiber taper used as the near-field coupling device was fabricated outside the purging system using the heat and pull method.²⁰ The fabrication was done on a rail system so that it could be transported into the purging chamber without breaking the fragile fiber taper. The reason behind using the rail system instead of fabricating directly within the purging chamber was that the stepper motor cannot be placed within the chamber making it more difficult to control the tension within the fiber taper during fabrication. The lack of tension control could lead to large inconsistencies when creating the fiber taper, and often resulted in huge signal losses when the system was cooled to cryogenic temperatures, sometimes to the point where no signal could be detected by the photo detector. Figure 1 shows the present experimental setup.

The purging chamber and working cell were added to the present experimental setup so that cryogenic temperatures could be reached and the WGM sensor would not undergo any frosting. The purging chamber was built from PVC boards. The chamber base has regularly spaced threaded holes allowing for the mounting of the fiber taper rail system, stages, and posts, as required. The walls of the chamber are lined with a number of threaded ports allowing for whatever gauges and liquid/gas/electrical/optical inlets and outlets the experiment may require. For example, there are two ports used for the optical fiber input/output, one port used for a vacuum gauge, one port attached to a roughing

pump, one port used for the liquid nitrogen (LN2) inlet, one port used for the nitrogen gas inlet, one port used for electrical inputs, and one port used for thermocouple inlets, in the present setup. The top of the chamber consists of an O-ring to allow for a vacuum seal, and the PVC lid is attached to the chamber using a number of metal clamps.

The working cell was designed for the purpose of cooling the electrical component to cryogenic temperatures, as well as, to insulate the environment around the WGM resonator eliminating any significant temperature fluctuations caused by air currents around the resonator. To achieve this the working cell was fabricated out of a hollow aluminum bar and covered with insulation. The inside of the aluminum is used as an LN2 reservoir. Two copper rods are inserted into the LN2 reservoir. The electrical component is threaded through holes in these rods allowing them to act as cold fingers. Two steel screws are also threaded through the aluminum, the electrical component is tied around these two screws, and they can be adjusted to control tension in the electrical component as well as alignment between the WGM sensor and the fiber taper. A combination of electrical tape and thermal paste is used to electrically insulate the electrical component from the rest of the system, while keeping it in good thermal contact. The WGM sensor is surrounded by a larger solid piece of copper that also reaches into the LN2 reservoir. This piece of copper has two perpendicular channels machined into it to allow both the fiber taper and electrical component to be positioned inside of it, the purpose of this copper is to increase the thermal inertia around the resonator allowing a more stable thermal environment at cryogenic temperatures. A second thin walled copper cylinder surrounds this piece of copper; this thin walled copper has 4 slits roughly one millimeter thick cut into it. These slits line up with the channels in the larger copper cylinder and prevent any air currents from affecting the thermal stability around the WGM sensor. A PDMS lid covers the larger copper cylinder. An additional aluminum case is placed around the entire electrical component, copper, and aluminum rods, and covered with a PDMS lid, to allow for additional insulation of the cryogenic environment, several small holes were

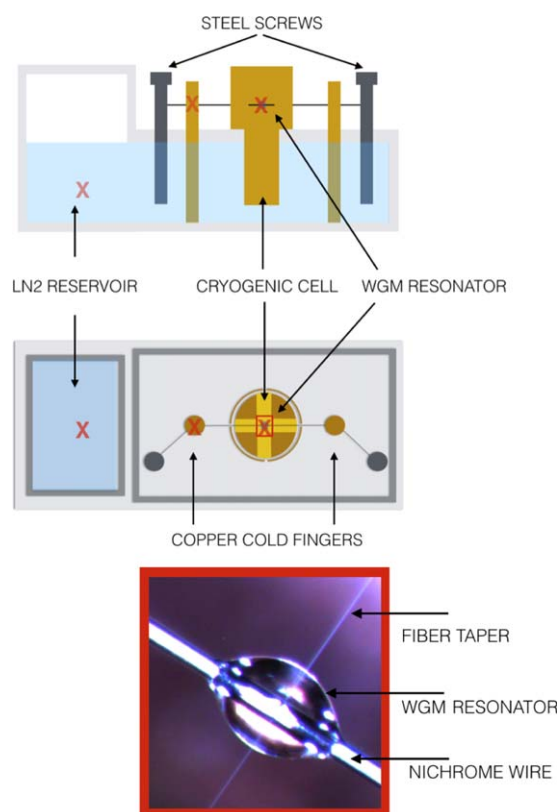


FIGURE 2 Cross-sectional and top views of the cryogenic cell, the red X's represent thermocouple locations. Inside the red box is a photo showing fiber-resonator coupling. [Color figure can be viewed in the online issue, which is available at wileyonlinelibrary.com.]

drilled into this casing so that thermocouples can be used to monitor the temperatures of the cold fingers and WGM sensor environment. Figure 2 shows both a cross section and a top view of the working cell.

PDMS was chosen instead of fused silica or poly(methyl methacrylate) (PMMA) as the WGM resonator medium primarily because of its relatively low temperature required for fabrication, which will not damage the microelectronic components/devices to be coated onto. PDMS-coated WGM resonators can be fabricated at room temperature using techniques put forth in Frenkel et al.,²⁹ whereas, fused silica WGM resonators require high temperatures (>1700 °C) that would ignite the nichrome wire used as the electrical component, and would cause failure in most other materials that could be used to replace the nichrome, such as tungsten. PMMA requires temperatures above 100 °C that may adversely affect many electronic components. This does have some drawbacks. PDMS will have a lower Q -factor than a fused silica resonator due to intrinsic material properties and surface smoothness. PDMS has, to the author's knowledge, not been explored as a WGM resonator at cryogenic temperatures, therefore, it was unknown if a PDMS resonator would support WGMs in the desired temperature range.

Finally, though the mechanical, electrical, optical, and thermal properties of some polymers and metals have been studied at low temperatures, the specific properties within our temperature range for both nichrome and PDMS were not available in the literature.³⁰ Therefore, where possible, we used our system to explore these properties and their relationships.

RESULTS AND DISCUSSION

Chamber Testing

Before experiments with WGM sensors could take place, the low temperature capabilities and stability of the working cell needed to be determined. It was found that when the LN2 reservoir was filled, normally taking about 4 L of LN2 slowly poured through the LN2 outlet over the course of 20–25 min that a stable <90 K could be reached in the cold fingers, and a stable temperature <100 K could be reached within the cryogenic working cell. The LN2 reservoir was capable of keeping the system at these low temperatures for approximately 10 min before it was depleted enough to allow the system to warm. Figure 3 shows the temperatures curves of the LN2 reservoir, one cold finger, and within the cryogenic cell during the cooling, stable, and warming processes. The positions of these thermocouples are marked with red X's in Figure 2. It can also be seen that a vacuum was introduced into the system shortly after the LN2 reservoir was filled. The intention of this vacuum was to cause a phase change of the LN2 into solid nitrogen dropping its temperature an additional 5–10 K. It can be seen that both the LN2 reservoir and the cold finger responded to this vacuum with temperature drops, but that the temperature within the cryogenic cell began to warm slightly under the vacuum. We attribute this warming within the cryogenic cell to the influx of the warmer surrounding air contained within the purging chamber that will occur because of the pressure differential created by the roughing pump. This warming could be overcome with a larger LN2 reservoir that would give

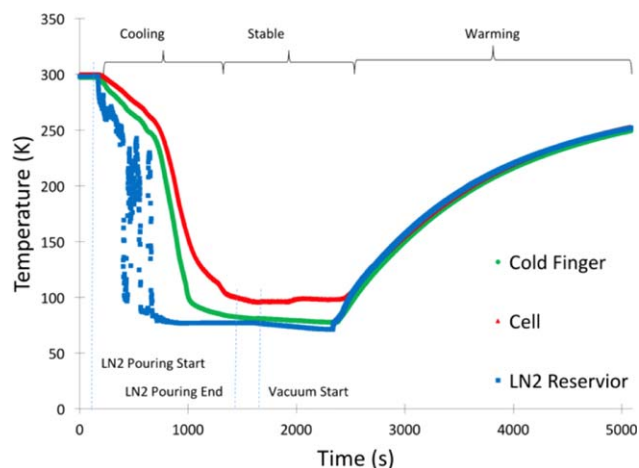


FIGURE 3 Temperature profiles of various parts of the working cell. [Color figure can be viewed in the online issue, which is available at wileyonlinelibrary.com.]

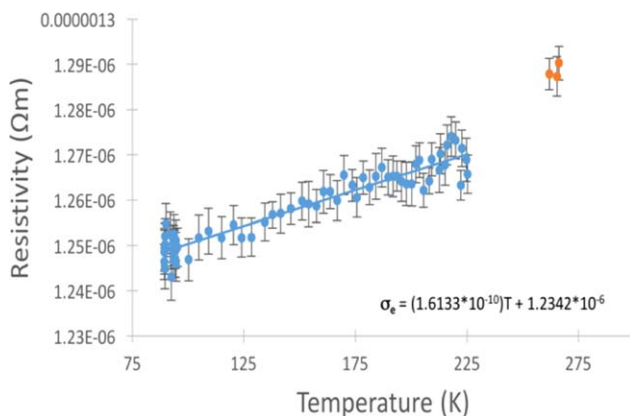


FIGURE 4 Resistivity of nichrome vs temperature changes. [Color figure can be viewed in the online issue, which is available at wileyonlinelibrary.com.]

the system more time to reach equilibrium with the solid nitrogen under vacuum, but such a reservoir is currently incompatible with the dimensions of our purging chamber; therefore, no vacuum was used when testing the WGM sensors. It was also found that if the system was cooled and left to warm without any vacuum the temperature within the cryogenic cell changed <1 K throughout the stable region of the temperature profile.

Determination of Nichrome Resistivity

After the temperature profile within the cryogenic cell was understood a bare nichrome wire was placed within the cell so that its electrical resistivity could be determined within the cryogenic temperature regime. Utilizing a 4-point probe method, in conjunction with our working cell, the electrical resistivity of a nichrome was experimentally determined in the cryogenic temperature regime.³¹ Two probes are connected to the nichrome wire and used to introduce a constant direct current; another two probes are connected to the current-carrying portion of the wire and used to monitor the electrical resistance. The electrical resistivity of the wire can then be calculated using Ohm's Law. Figure 4 shows the electrical resistivity of the nichrome wire as the temperature increases from cryogenic toward room temperature. At room temperature the resistivity of nichrome was reported to fall between 1.1 and 1.5 $\Omega\mu\text{m}$.^{32,33} A value of $1.288 \pm 0.08 \Omega\mu\text{m}$ was measured in the current experiments. A decrease in resistivity is seen with a decrease in temperature, at cryogenic temperatures the resistivity of nichrome reaches about 97% of the room temperature value. The cryogenic value (95–140 K) of resistivity was found to be $1.261 \pm 0.08 \Omega\mu\text{m}$ for the wire used during the dynamic temperature testing. A linear fitting of the data gave the following correlation

$$\sigma_e = (1.6133 \times 10^{-10})T + 1.2342 \times 10^{-6} \quad (1)$$

where T is absolute temperature and σ_e is the electrical resistivity. This correlation was obtained in the cryogenic to low temperature range from 90 to 225 K.

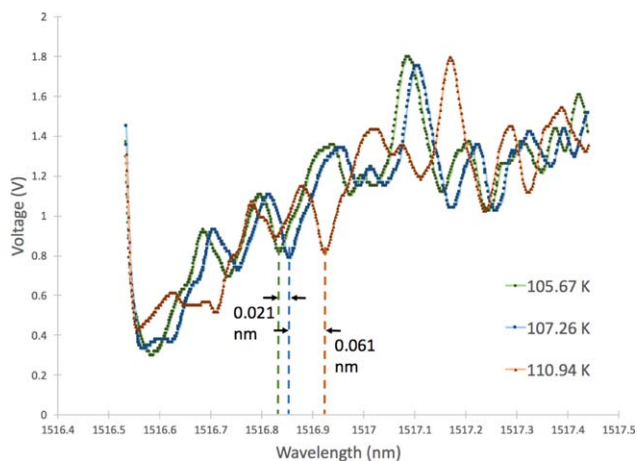


FIGURE 5 WGM resonance spectra and shifts at three different temperatures. [Color figure can be viewed in the online issue, which is available at wileyonlinelibrary.com.]

WGM Calibration and Analysis

The first WGM experiments conducted were meant to determine if PDMS was capable of supporting WGM resonance at cryogenic temperatures. The working cell was cooled as previously described. Prior to the cooling of the working cell the purging chamber underwent a nitrogen gas purging. The purpose of this nitrogen purge is to remove any humidity contained within the chamber, and thus prevent any frosting that could occur on the resonator or fiber taper. If frosting were allowed to occur, it would affect the coupling between the resonator and taper either decoupling the system completely or reducing the signal received by the photodetector beyond detection.

While the system is being cooled after the nitrogen purge, the WGM signal can be watched on a local computer. A decrease in signal was often seen accompanying the system cooling. This decrease in signal can most likely be attributed to tension created in the fiber taper due to the thermal strain placed on it. The signal loss was normally in the order of ~20 dB and could be easily made up for with the gain of the photodetector, unlike the signal loss that occurred without a nitrogen purge. Additionally, a drop in resonator quality was also seen as the system was cooled. This drop was normally smaller than an order of magnitude and may be a result of changes in the optical and surface properties of the PDMS as it is cooled. At cryogenic temperature Q -factors of the PDMS resonators were often found around $\sim 1.5 \times 10^5$ down from values around $\sim 5 \times 10^5$ at room temperature. Once the system reached a stable temperature data could be collected as the system warmed naturally. Using the same procedure as discussed in Frenkel et al.,²⁹ data were collected at regular intervals throughout the warming of the system.

Figure 5 shows the resonance spectra at three different temperatures. The two shifts in resonance from the temperature changes can be easily seen in this figure, with the larger temperature difference corresponding to a larger resonance

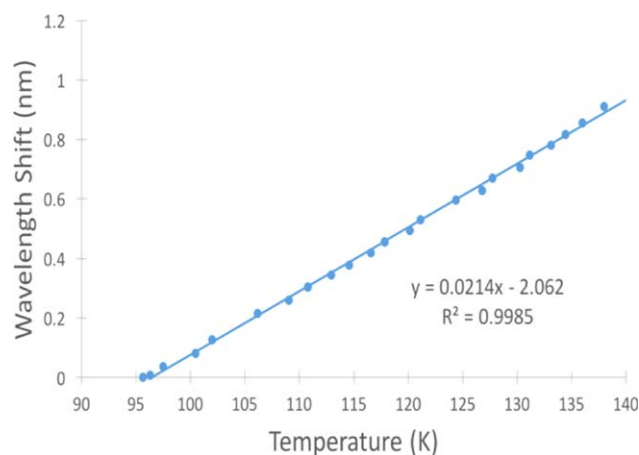


FIGURE 6 A single calibration showing temperature vs wavelength shifts from 95 to 140 K. [Color figure can be viewed in the online issue, which is available at wileyonlinelibrary.com.]

shift. Once the data are collected across the desired temperature regime it could be used to calibrate the sensitivity of the PDMS WGM resonator.

Figure 6 shows a single calibration curve for a 639- μm diameter PDMS shell resonator, fabricated by allowing a PDMS droplet (10:1 weight ratio base to curing agent) to cure onto the nichrome wire (127 μm in diameter). The curve shows a linear relationship ($R^2 = 0.9985$) between temperature shifts and wavelength shifts from temperature of approximately 95 to 140 K. The value of the sensitivity is 0.0214 nm/K. This value is of interest because it demonstrates a clear difference from the expected room temperature sensitivity. Frenkel et al.²⁹ showed that a PDMS-coated resonator of this size, at room temperature should have a sensitivity between 0.1 and 0.15 nm/K. Therefore, it is clear that the optical and thermal properties of the PDMS and nichrome have changed when cooled to cryogenic temperatures. A number of different WGM resonators were calibrated using this technique so that

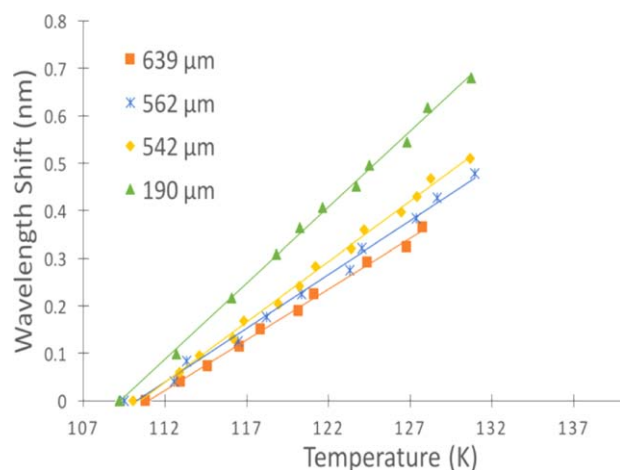


FIGURE 7 Calibration curves for four resonator of varying diameter. [Color figure can be viewed in the online issue, which is available at wileyonlinelibrary.com.]

TABLE 1 Sensitivity of Four Different PDMS Shell Sensors

Shell Diameter (μm)	Sensitivity (nm K^{-1})	Coefficient of Determination
190	0.032	0.9974
542	0.025	0.9964
562	0.023	0.9937
639	0.021	0.9985

the effects of the coated PDMS shell diameter on temperature sensitivity could be examined.

Figure 7 shows the calibration curves of 4 different PDMS resonators coated to the same nichrome wire, and Table 1 lists the sensitivities and correlation coefficients of each resonator. It should be noted that the temperature region of Figure 7 was chosen because it had the best overlap between all the four resonators. Calibration of the resonators was done as low as 95 K for most resonators tested. The temperature caused WGM wavelength shifts that occur within the resonator can be explained as follows:

$$\frac{d\lambda}{dT} = \lambda_0 \left(\frac{1}{n} \frac{dn}{dT} + \frac{1}{D_2} \frac{dD_2}{dT} \right) = \lambda_0 \left(\frac{1}{n} \alpha + \beta_{\text{eff}} \right) \quad (2)$$

where λ_0 is the incident laser wavelength (1516 nm), α is the PDMS thermal optical coefficient, D_2 is the diameter of the PDMS resonator, n is the index of refraction of the PDMS, and T is temperature. β_{eff} is the effective thermal expansion coefficient based on both the PDMS coating and nichrome core given below.³⁴

$$\beta_{\text{eff}} = \beta_2 - \left(\frac{D_1}{D_2} \right)^2 \frac{(1+\nu_2)/2E_2}{[(1+\nu_2)/2E_2] + [(1-\nu_1)/E_1]} (\beta_2 - \beta_1) \quad (3)$$

where the subscripts 1 and 2 represent the core (nichrome) and coating (PDMS), respectively, E represents the Young's modulus, and ν represents the Poisson ratio. As expected there is a relationship between the diameter of the coated resonator and its sensitivity, but the results differ greatly from what was seen at room temperature. At room temperature the negative thermal optical coefficient of PDMS caused a negative sensitivity when the PDMS coatings were thin; as the coating diameter increased the magnitude of the sensitivity increased eventually reaching a critical diameter where the WGM resonance would be stable against temperature changes.²⁶ Once the PDMS coating diameter increased beyond the critical diameter the WGM sensitivity became positive and continued to increase until reaching an asymptotic value. In the cryogenic temperature regime, however, we see a very different effect of PDMS coating thickness on sensitivity. The sensitivity value is positive even at the thinnest coating thickness considered (190 μm in diameter equals to a PDMS layer of 31.5 μm thick). Additionally, the magnitude of sensitivity decreases as the coating thickness increases, the opposite of what was seen at room temperature.²⁶ Without exact data on the thermal and optical

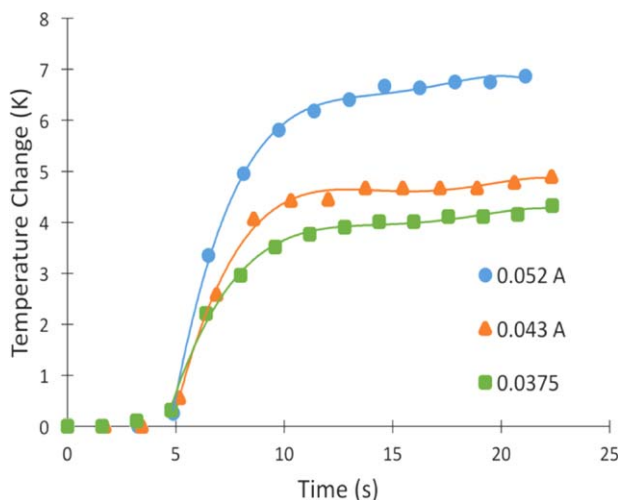


FIGURE 8 Real-time temperature monitoring by a calibrated WGM resonator at three different electrical currents and fitting lines. [Color figure can be viewed in the online issue, which is available at wileyonlinelibrary.com.]

properties of both PDMS and nichrome at cryogenic temperature it is difficult to find an exact analysis for the relationship between coating thickness and resonator sensitivity, but we can put forth certain expectations of how these properties will differ from their room temperature values. The positive sensitivity at all temperature values leads us to believe that either PDMS takes on a positive thermal optical coefficient and/or that the overall sensitivity is dominated by the thermal expansion term in eq 2. To understand the sensitivity decrease with coating thickness increase we can adapt eq 2 into the following two limiting cases:

$$\frac{d\lambda}{dT} = \lambda_0 \left(\frac{1}{n} \alpha + \beta_1 \right) \quad (4a)$$

$$\frac{d\lambda}{dT} = \lambda_0 \left(\frac{1}{n} \alpha + \beta_2 \right) \quad (4b)$$

Equation 4a represents an extremely thin coating of PDMS while eq 4b represents a very thick coating. Since we are seeing the magnitude of WGM sensitivity decrease with an increase in PDMS coating thickness, eqs 4a and 4b imply that $\beta_{\text{nichrome}} > \beta_{\text{PDMS}}$. It should be noted that at room temperature $\beta_{\text{PDMS}} > \beta_{\text{nichrome}}$,²⁶ and that the magnitude of sensitivity increased with increasing PDMS thickness.

Dynamic Temperature Monitoring and Analysis

After calibrating a resonator, we were able to perform dynamic temperature monitoring by introducing an electrical current into the nichrome wire. Two probes are connected to the electrical wire between the steel screws and copper cold finger on both sides of the working cell allowing a current to travel along this component and introduce Joule heating into the system. The PDMS shell resonator can then be used to directly monitor the temperature of the heating wire in real time. Figure 8 shows the heating curves at three different currents (0.0375, 0.043, and 0.052 A). The electrical

current is introduced into the system after a few seconds after data acquisition begins, at which point we see the expected heating curve for a wire undergoing internal Joule heating. Again, without the thermal properties of PDMS and nichrome in this temperature range, we cannot conduct a full dynamic theoretical analysis of the heated system. On the other hand, a steady-state theoretical analysis can be performed by setting the internal energy generated within the wire to the energy dissipated to ambient by convection. A simple energy balance of the system yields the following equation:

$$\frac{4I^2 \sigma_e}{\pi D_1^2} = \pi D_2 h \Delta T \quad (5)$$

where I is the current, ΔT is the change in temperature, h is the convective heat transfer coefficient due to natural convection in the ambient, and σ_e is the electrical resistivity of the nichrome core, which is determined from the measurement shown in Figure 4. For the cryogenic temperature range 95–140 K, the averaged resistivity of the nichrome wire was found to be $1.261 \pm 0.08 \Omega \mu\text{m}$. The convective heat transfer coefficient was determined via Churchill and Chu's correlation for natural convection over a horizontal cylinder³⁵:

$$\frac{hD_2}{k} = \left\{ 0.6 + \frac{0.387 \text{Ra}_D^{1/6}}{\left[1 + (0.559/\text{Pr})^{9/16} \right]^{8/27}} \right\}^2 \quad (6)$$

In which, Pr is the Prandtl number, Ra_D is the Rayleigh number, and k is the thermal conductivity of the fluid. This approximation is valid for $10^{-5} < \text{Ra}_D < 10^{12}$. Both the Prandtl and Rayleigh numbers were calculated assuming a pure nitrogen gas environment at approximately 100 K. At this temperature and in this system $\text{Pr} = 0.76$ and the Rayleigh number is found to be between approximately 0.15 and 0.28 depending on the temperature shift. Table 2 compares the temperature rises in steady state between theoretical analysis and experimental measurement. The error for the theoretical prediction is based on error propagation from the measurements of the core and coating diameters, as well as, the measurements of electrical resistivity and current. Our experimental and theoretical data are in excellent agreement.

Lastly, it should be noted that the Q -factors of the PDMS shell/bead resonators in this study were found to be high 10^4 to low 10^5 when at cryogenic temperatures. This implies that our systems ultimate temperature resolution under our

TABLE 2 Comparison of Experimentally Determined and Theoretically Predicted Temperature Rises at Steady State

Current (A)	Experimental ΔT (K)	Analytical ΔT (K)	Difference (K)
0.0375	4.11 ± 0.12	3.84 ± 0.52	0.27
0.043	4.83 ± 0.13	4.86 ± 0.64	0.03
0.052	6.79 ± 0.14	6.76 ± 0.86	0.03

current data acquisition system will be between 0.1 and 0.01 K following the analysis introduced by Ma et al.²⁰ The only way to improve this would be to increase the Q -factor of the resonators either through new fabrication techniques or by using a different resonator material.

CONCLUSIONS

The results of this study demonstrate for the first time that PDMS-coated microresonators will support WGM resonance at cryogenic temperatures, and that these polymeric composite sensors can be used to accurately monitor on-chip temperature changes in cryogenic environment. We see from this study that the thermal and optical properties of PDMS and nichrome are affected by the dramatic change in temperature that occurs when going from a room temperature environment to a cryogenic one.

We built a simple cryogenic system capable of reaching a stable temperature down to 95 K. At this temperature the electrical resistivity of nichrome wire was experimentally measured, and the PDMS-coated sensors were calibrated to obtain their sensitivities. The polymeric sensors achieved Q -factors on the order of 10^5 , resulting in a fine temperature resolution 0.01 K at the cryogenic regime. The temperature rising in the current-carrying wire was monitored by the coated PDMS sensor, such that onsite dynamic information was acquired. The comparison of measurement with theoretical analysis showed an excellent agreement.

ACKNOWLEDGMENTS

This material is based upon work supported by the National Science Foundation under grant no. CBET-1067141. We would like to thank Marlon Avellan, John Petrowski, and Joseph Vanderveer whose assistance was instrumental to all the machining needed to fabricate the purging chamber and working cell. M. Frenkel appreciates the support of an NJSGC graduate fellowship in 2014.

REFERENCES AND NOTES

- 1 S. L. McCall, A. F. J. Levi, R. E. Slusher, S. J. Pearton, R. A. Logan, *Appl. Phys. Lett.* **1992**, *60*, 289–291.
- 2 N. Dubreuil, J. C. Knight, D. K. Leventhal, V. Sandoghdar, J. Hare, V. Lefèvre, *Opt. Lett.* **1995**, *20*, 813–815.
- 3 A. Serpengüzel, G. Griffel, S. Arnold, *Opt. Lett.* **1995**, *20*, 654–656.
- 4 M. Gorodetsky, A. Savchenkov, V. Ilchenko, *Opt. Lett.* **1996**, *21*, 453–455.
- 5 M. Cai, O. Painter, K. J. Vahala, *Phys. Rev. Lett.* **2000**, *85*, 74–77.
- 6 S. Parkins, T. Aoki, *Phys. Rev. A* **2014**, *90*, 053822.
- 7 H. C. Tapalian, J. P. Laine, P. A. Lane, *IEEE Photon. Tech. Lett.* **2002**, *14*, 1118–1120.
- 8 L. Lui, R. Kumar, K. Huybrechts, T. Spuesents, G. Roelkens, E. Geluk, T. Vries, P. Regreny, D. V. Thourhout, R. Baets, G. Morthier, *Nat. Photon.* **2010**, *4*, 182–187.
- 9 A. R. Ali, T. Ioppolo, V. Otugen, M. Christensen, D. MacFarlane, *J. Polym. Sci. Part B: Polym. Phys.* **2014**, *52*, 276–279.
- 10 S. Arnold, M. Khoshshima, I. Teraoka, S. Holler, F. Vollmer, *Opt. Lett.* **2003**, *28*, 272–274.
- 11 H. Quan, Z. Guo, *Nanotechnology* **2007**, *18*, 375702.
- 12 A. M. Armani, R. P. Kulkarni, S. E. Fraser, R. C. Flagan, K. J. Vahala, *Sci.* **2007**, *317*, 783–787.
- 13 F. Vollmer, S. Arnold, *Nat. Methods* **2008**, *5*, 591–596.
- 14 L. He, S. K. Ozdemir, J. Zhu, W. Kim, L. Yang, *Nat. Nanotechnol.* **2011**, *6*, 428–432.
- 15 V. Dantham, S. Holler, V. Kolchenko, Z. Wan, S. Arnold, *Appl. Phys. Lett.* **2012**, *101*, 043704.
- 16 L. Huang, Z. Guo, *Nanotechnology* **2012**, *23*, 065502.
- 17 Q. Ma, L. Huang, L., Z. Guo, *Meas. Sci. Technol.* **2010**, *21*, 115206.
- 18 T. Ioppolo, M. Kozhevnikov, V. Stepaniuk, M. Otugen, V. Sheverev, *Appl. Opt.* **2008**, *47*, 3009–3014.
- 19 G. Guan, S. Arnold, V. Otugen, *AIAA J.* **2006**, *44*, 2385–2389.
- 20 Q. Ma, T. Rossmann, Z. Guo, *J. Phys. D: Appl. Phys.* **2008**, *41*, 245111.
- 21 Q. Ma, T. Rossmann, Z. Guo, *Meas. Sci. Technol.* **2010**, *21*, 025310.
- 22 D. V. Strelakov, R. J. Thompson, L. M. Baumgartel, I. S. Grudin, N. Yu, *Opt. Express* **2011**, *19*, 14495.
- 23 W. Xu, M. G. Allen, *J. Polym. Sci. Part B: Polym. Phys.* **2013**, *51*, 1505–1512.
- 24 S. Gupta, T. Mizunami, T. Yamao, T. Shimomura, *Appl. Opt.* **1996**, *35*, 5202–5205.
- 25 J. S. Moore, S. S. Xantheas, J. W. Grate, T. W. Wietsma, E. Gratton, A. E. Vasdekis, *J. Polym. Sci. Part B: Polym. Phys.* **2015**, *54*, 98–103.
- 26 L. He, Y. F. Xiao, C. Dong, J. Zhu, V. Gaddam, L. Yang, *Appl. Phys. Lett.* **2008**, *93*, 201102.
- 27 C. H. Dong, L. He, Y. F. Xiao, V. R. Gaddam, S. K. Ozdemir, Z. F. Han, G. C. Guo, L. Yang, *Appl. Phys. Lett.* **2009**, *94*, 231119.
- 28 B. Li, Q. Wang, Y. Xiao, X. Jiang, Y. Li, *Appl. Phys. Lett.* **2010**, *96*, 251109.
- 29 M. Frenkel, M. Avellan, Z. Guo, *Meas. Sci. Technol.* **2013**, *24*, 075103.
- 30 O. Yano, H. Yamaoka, *Prog. Poly. Sci.* **1995**, *20*, 585–613.
- 31 F. M. Smits, *Bell Sys. Tech. J.* **1958**, *37*, 711–718.
- 32 I. Robertson, *Electronics for Electricians and Engineers*; Industrial Press: New York, **1987**; 34.
- 33 J. S. Faughn, S. A. Raymond, *College Physics*; Thomson Learning Inc.: Pacific Grove: **2003**; p 538.
- 34 R. R. Tummala, A. L. Friedberg, *J. Appl. Phys.* **1970**, *41*, 5104–5107.
- 35 A. Bejan; *Convection Heat Transfer*; Wiley: Hoboken, **2004**; Edition 3; p 221.